Measuring the thermal conductivity of membrane and porous transport layer in proton and anion exchange membrane water electrolyzers for temperature distribution modeling

Robert Bock [a,b], Håvard Karoliussen [a], Frode Seland [b], Bruno G. Pollet [a], Magnus Skinlo Thomassen [c], Steven Holdcroft [d], Odne S. Burheim [a,*]

[a] Department of Energy and Process Engineering, Norwegian University of Science and Technology, NO-7491 Trondheim, Norway
[b] Department of Materials Science and Engineering, Norwegian University of Science and Technology, NO-7491 Trondheim, Norway
[c] Sustainable Energy Technology, SINTEF Energy Research, NO-8608 Mo i Rana, Norway
[d] Department of Chemistry, Simon Fraser University, Burnaby, B.C. V5A 1S6, Canada

ARTICLE INFO

ABSTRACT

Water electrolyzers that use a membrane electrolyte between the electrodes are a promising technology towards mass production of renewable hydrogen. High power setups produce a lot of heat which has to be transported through the cell, making heat management essential. Knowing thermal conductivity values of the employed materials is crucial when modeling the temperature distribution inside an electrolyzer. The thermal conductivity was measured for different titanium-based porous transport layers (PTL) and a partially methylated Hexamethyl-p-Terphenyl Polybenzimidazolium (HMT-PMBI-Cl$^-$) membrane. The four titanium-based sintered transport layers materials have thermal conductivities between 1.0 and 2.5 $\pm$ 0.2 WK^{-1}m^{-1} at 10 bar compaction pressure. The HMT-PMBI-Cl$^-$ membrane has a thermal conductivity of 0.19 $\pm$ 0.04 WK^{-1}m^{-1} at 0% relative humidity at 10 bar compaction pressure and 0.21 $\pm$ 0.03 WK^{-1}m^{-1} at 100% relative humidity ($\lambda = 12$ water molecules per ion exchange site at room temperature) at 10 bar compaction pressure. Combining the determined thermal conductivity values with data from the literature, 2D thermal models of a proton exchange membrane water electrolyzer (PEMWE) and an anion exchange membrane water electrolyzer (AEMWE) were built to evaluate the temperature distribution in the through-plane direction. A temperature difference of 7 –17 K was shown to arise between the center of the membrane electrode assembly and bipolar plates for the PEMWE and more than 18 K for the AEMWE.

---

* Corresponding author.
E-mail address: burheim@ntnu.no (O.S. Burheim).

Introduction

The possible success of the hydrogen economy is very dependent on viable and affordable technologies that enable mass production of hydrogen on the basis of renewable energies [1]. Hydrogen with a very high purity of close to 100% can be obtained through the process of water electrolysis, the electrochemical conversion of water to hydrogen and oxygen [2]. With the growing availability of renewable energy in many countries the chances for electrolytic hydrogen won from these sources increases. It can then pose as an energy storage medium and an energy carrier, helping to balance the intermittency of renewable energy sources and to deliver this renewable energy where it might otherwise not be available [3].

Being the most energy-dense chemical fuel (33 kWh kg^{-1}) hydrogen is well suited for the transportation sector [4], and it is also well suited for making less dense liquid hydrocarbon fuels from remaining renewable CO_2 surplus streams [5].

The electrolytic process can be reversed to produce current, heat and water when demands peak and surplus electricity is needed. This conversion of chemical energy into electrical energy goes by means of a fuel cell. For some applications such a device that works both as a fuel cell and an electrolyzer is desirable as it can function as a local energy buffer and help to stabilize power demands.

Electrolysis as a technology enables the ideas of Power-to-Gas (PtG) and Power-to-Liquids (PtL) [6]. The idea is that the growing amount of renewable energy sources also introduces a high uncertainty of when power is available, whilst the demand for power is predictable. To cope with this, power capacities have to be slightly overplanned in terms of energy type, location and flexibility. At times, there will be more power available than needed. This surplus power can be converted into hydrogen which can be injected into the natural gas network, thus PtG, instead of going to waste. In a succeeding step this hydrogen may even be converted to a liquid fuel by Fischer-Tropsch synthesis of H_2 and CO_2, hence PtL [7]. The storage capacities that can be realized in this way are enormous and can even be used to compensate for seasonal fluctuations in power production through renewables [8]. Several studies have been published that showcase and discuss pilot projects that include renewable energy sources, production of electrolytic hydrogen, hydrogen storage and a fuel cell in one location to demonstrate the capabilities of combining these technologies [9,10]. Large scale introduction of such systems to balance entire countries' grids has been discussed for the Great Britain and Spain, for instance Refs. [11,12].

To further develop and optimize the electrolysis technology, the understanding and management of the heat used in the process is a crucial factor. An increase in operating temperature will lead to a reduction of ohmic and activation losses in the cell, due to the membrane having higher ionic conductivity and also due to faster reaction kinetics [13]. This will increase the efficiency of the electrolysis reaction [14]. The desire to maximize operating temperature locally requires a proper prediction of the actual temperature distribution in the cell. There exist substantial temperature gradients that have

been neglected in literature so far. Determining the thermal conductivity of the subcomponents in the electrolyzer helps to understand and manage the reaction kinetics as well as ageing and degradation within it.

The key components of an electrolyzer are bipolar plates (BPPs) to supply water, flow field meshes that are used as fluid distributor, the membrane electrode assembly (MEA), and porous transport layers (PTL). The PTLs are located between the meshes and the catalyst coated membrane (CCM), see Fig. 1. Their function is to supply water, remove the produced gas, conduct electricity and transfer heat.

Water electrolysis

The technology of electrolysis has been around for almost one hundred years commercially. Water electrolysis has been performed on an industrial scale in the megawatt range and is thus well-known and established. Commercially three water electrolysis technologies dominate: proton exchange membrane water electrolysis (PEMWE), alkaline water electrolysis, and solid oxide water electrolysis [4,15]. In this work we are exploring PEMWE and how its advantages may be applied to an alkaline environment by using an anion exchange membrane (AEM) instead of the PEM.

Proton exchange membrane water electrolysis
The major advantage of the PEMWE technology is the use of a membrane as a separator between the electrodes. It can be very thin, below 50 μm, and as such electric resistance is minimized. The electrodes are mounted on each side of the membrane, creating an MEA. Product gas bubbles are emitted on each side and removed by the water in the flow field channels. On the hydrogen side, water could be omitted, as it is only needed on the anode side, resulting in pure hydrogen gas streaming out of the cell. Apart from the low electrical resistance, PEMWE also offers very good kinetics for the hydrogen evolution reaction (HER). The Tafel overpotential is almost negligible and can be considered constant, solely depending on the catalyst loading.

A challenge for PEMWE pose the conditions on the anode side where the oxygen evolution reaction (OER) takes place. When using platinum to catalyze this reaction the potential must not exceed 0.242 V$_{NHK}$ as platinum will resolve actively beyond that. As higher potentials are desirable, research efforts are put into developing a ruthenium oxide based catalyst, where ruthenium (Ru) is mixed with similar but more expensive materials like iridium, rhodium or osmium who are less active but more stable than Ru. This will stabilize Ru at the cost of being less active [16,17].

Anion exchange membrane water electrolysis
Alkaline electrolysis is the technology that was introduced to the industry around 100 years ago. In search of electrode materials that would not dissolve at the high potentials of above 1.23 V$_{SHE}$ it was found that high pH values lower the anode potential. This resulted in the use of alkaline solution as electrolyte which in turn enabled readily available nickel to be used as electrode material. Traditionally a diaphragm was used as a barrier for the gas bubbles from both electrodes while still allowing the OH$^-$ ions to migrate from cathode to
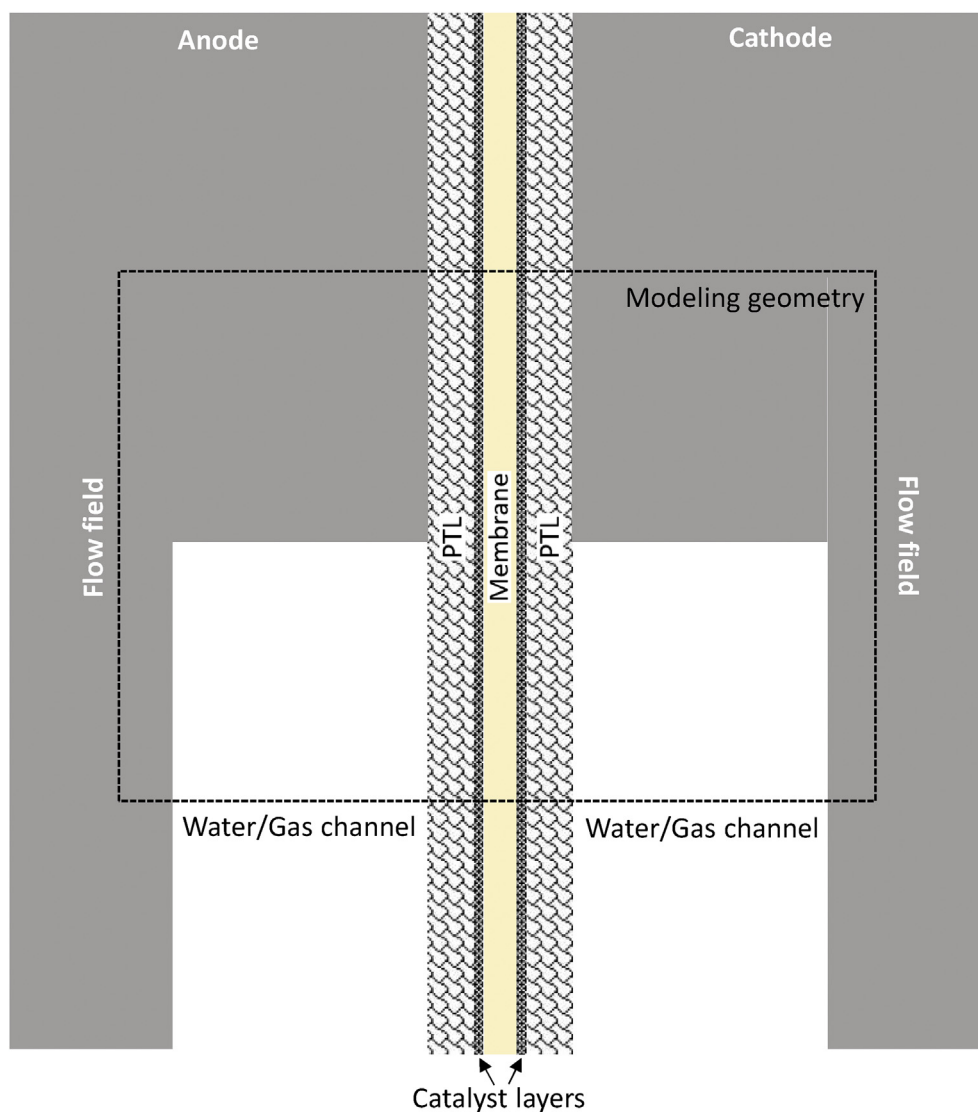
Fig. 1 – **Simplified general setup of an electrolyzer, part of the whole geometry.**

anode. These diaphragms are around 10 mm thick and have a specific ohmic resistance of around 1 Ωcm^2 which poses a drawback for the technology [4]. It is here the idea of AEM water electrolysis (AEMWE) bears considerable potential for improvement. If a membrane that separates the product gases while allowing hydroxide ions to pass through could be employed in an alkaline electrolyzer, the ohmic resistance of this system would drop significantly due to a hydroxide conductivity of around 0.02 Scm^{-1}. Additionally, the membrane has a thicknesses of 0.1 mm and below which results in a resistance several orders of magnitude lower than the original diaphragms [18]. Such an electrolyzer would combine the advantages of an alkaline electrolyte, permitting less expensive nickel electrodes, and an ion exchange membrane as separator with low resistance.

Heat sources and thermal conductivity

The endothermic electrochemical reaction of producing hydrogen and oxygen from electricity requires heat to convert the electrical work into chemical energy [2]. In an electrolyzer this heat is usually supplied by ohmic heating in the electrolyte of the cell. This leads to temperature gradients in the through-plane direction inside the electrolyzer. The heat needs to be transported from where it is produced to where it is used and excess heat needs to be removed via the flow channels. To give a correct estimation of this process, thermal conductivities of the materials involved are needed. To our knowledge no studies have been published that report thermal conductivity of the materials involved in these temperature gradients, except for studies on Nafion® membranes [19] and possibly relevant PEMFC catalyst layers [20].

The necessary overpotentials at both electrodes to overcome activation energy barriers increase the heat production for a given current further.

Thermal models

It is of great importance to understand the thermal behaviour of electrolyzers for different designs and under the various

operating conditions to be able to accurately predict the temperature distribution in new electrolyzer designs. Because experimental determination of temperature distribution is invasive and associated with great cost one turns to thermal modeling to quickly cover many different parameter variations and make sufficient predictions. Models accounting for thermal gradients in water electrolyzers are absent in the literature, no published efforts have come to our attention. There exist some models of alkaline water electrolysis, but they are focused mainly on overpotentials and assume isothermal conditions through the electrolyzer. There are a number of studies on the effect of temperature on the performance of alkaline water electrolyzers. Over 30 years ago, Miles et al. found that increasing the operating temperature of an alkaline electrolysis cell with nickel-based electrodes allowed for increased electrolyte ionic conductivity and enhanced electrode surface kinetics. They also found that the main disadvantage of increasing the cell temperature was the reduced durability of cell materials which came into contact with the corrosive electrolyte [21]. Similar findings were made by Bailleux et al. in their two year running of a test plant. They found that operation at 150 °C and 10 kA m^{-2} improved the overall voltage by 120 mV, as compared to 120 °C operation at the same current density. In other words, the improvement was 4 mV °C^{-1} [22]. The influence of temperature on energy consumption was studied by Stojic et al., they found positive effects of a rise in temperature on energy consumption. In their study they introduced ionic activators into the electrolyte to reduce the activation energy [23]. The effect of water electrolysis temperature on PEMWE was studied by Maeda et al. [24]. They showed that an increase in water temperature from 30 °C to 80 °C lowered the needed electrode potential for 1.6 Acm^{-2} from 2.3 V to 1.8 V [24]. These studies show that knowing and controlling the exact temperature in a water electrolyzer is of utmost importance.

Hug et al. presented the simulation model SIMELINT (SIMulation of ELectrolyzers in INTermittent operation) in 1993, which was able to calculate thermal behaviour, cell voltage, gas purity and efficiency of an alkaline electrolyzer. It was intended to help with the design and optimization of electrolyzers and for control strategies of intermittent electrolyzer operation [25]. A mathematical model of an alkaline water electrolyzer was built in the work of Ulleberg [26]. His model considers heat transfer theory and included a dynamic thermal model which was intended for use in integrated hydrogen energy system simulations. A 1-year simulation of a photovoltaic-hydrogen system was performed [26]. An experimental study with mathematical modeling on the thermal performance of a commercial electrolyzer was performed by Dieguez et al. [27]. They included a study of the spatial variation of the temperature inside the electrolyzer and conclude with a relative homogeneity of the temperatures on the several components and the absence of important temperature gradients. Their approach explicitly assumed that temperature gradients within the electrolyzer can be neglected, i.e. they did not consider temperature gradients that may occur within the cells themselves. Their main finding is that different DC current profiles of the power supply device have a remarkable effect on the thermal performance of the electrolyzer [27]. More recently, Abdin et al.

published an enhanced one-dimensional model of an alkaline electrolyzer based on linked modular mathematical models in Simulink® 28. It is a tool for understanding the overall equilibrium electrolyzer cell performance and takes into account the bubble effects. Employing this model they demonstrated how the exchange current densities of the anode and cathode affect the polarization curve differently at low and high cell current densities [28].

PEMWEs have also been studied and modeled. A simple model based on Butler–Volmer kinetics for electrodes and transport resistance in the polymer electrolyte was built and reported by Choi et al., showing that the high anode overpotential is a limiting factor for the electrolysis cell [29]. A 20-cell proton exchange membrane electrolyzer stack was modeled by Harrison et al. to find an expression to predict the polarization curve of a commercial electrolyzer. They calculated the membrane conductivity from their experimental data 0.075 Scm^{-1} [30]. Lebbal et al. reported an analytic model that consists of a steady-state electrical model and a linear dynamic thermal model of a PEMWE to improve the monitoring approach of such systems. It is intended to be used for the detection and isolation of faults on actuators, on sensors or on the electrolyzer system itself [31]. Another dynamic model of a PEMWE system based on MATLAB/Simulink® was proposed by Awasthi et al. [32]. They noticed that the ohmic overvoltage sharply increases while the activation overvoltage remains constant with an increase in current density, indicating that using low resistance electrolyte may improve electrolyzer performance [32]. A numerical investigation of PEMWE performance was used for examining the effect of anode catalyst on the cell performance by Kaya et al. [33]. Different parameters were examined and it was found that higher temperature, lower membrane thickness and lower current collector length increases the performance of a PEMWE [33].

All these studies assume an overall temperature in the entire electrolytic cell, they do not consider temperature gradients within the cell itself. Therefore, for the first time to the best of our knowledge, a simple 2D model is proposed in this study to illustrate the temperature gradients in different electrolyzer technologies and to show the influence of different thermal conductivities on these temperature gradients.

The aim of this study is to measure and report the thermal conductivity of different porous transport layer materials used in PEMWEs and of an anion exchange membrane developed for being used in an alkaline electrolyzer These values are subsequently used in a PEMWE and an AEMWE COMSOL heat distribution model. As a result, the temperature distribution in each cell can be studied, reported, and better understood.

Experimental

Titanium-based porous transport layers

The role of the PTL is to supply water for electrolysis, remove the product gases, conduct electricity, and transfer heat. Four different PTL types were used in this work, obtained from a

supplier of PEM electrolysers. All samples are made of titanium particles that were sintered before different surface treatments and coatings were applied [34]. It was not disclosed to us how the surface treatments were performed and what their intended functionality was. Table 1 gives an overview. A surface roughness measurement with White Light Interferometry (WLI) revealed that the Sinter-3 material has significantly rougher surface than the remaining three PTL materials.

A publicly available technical report on these materials includes SEM graphs of the surfaces as well as the edges of the four PTL materials [34], see Fig. 3.

The technical report suggests that different manufacturing strategies were used for the four different PTL materials. This resulted in pore size differences, as summarized in Table 2. The porosities of the four materials are very similar, but they differ significantly in their pore radii. Especially the Sinter-3 material stands out with much larger average and median pores than the remaining three PTL materials.

The samples were water cut to a diameter of 21 mm and then dried at 40 °C for at least 24 h to evaporate residual water. The thickness of the samples was around 1.5 mm. Fig. 2 shows the difference in appearance for the four PTL materials.

In the case of the Sinter-2 material a wet measurement was conducted as well. After the dry measurement, the samples were submerged in water at room temperature over night and stirred several times. Samples were weighed dry and wet to determine the amount of water contained in them. The dry samples had an average weight of 1.62 ± 0.03 g while the wet samples weighed in at 1.75 ± 0.02 g. On average the samples contained 0.12 ± 0.05 g of water.

Table 1 — Sinter materials surface treatment and surface roughness as measured with White Light Interferometry (WLI).

Material	Treatment and coating	RMS of surface roughness
Sinter-1	no treatment	11.3
Sinter-2	treated by oxalic acid	11.0
Sinter-3	Pt-coating method A	19.3
Sinter-4	Pt-coating method B	11.9

Anion exchange membrane

AEMs in alkaline water electrolyzers are developed to transport hydroxide ions. As mentioned, the prospects of using a membrane instead of a diaphragm lie in the significant reduction of thickness and thus in ionic resistivity. The alkalinity of the membrane also enables the use of non-noble-metal-based catalysts as compared to the acidic nature of Nafion® [18].

The membrane was prepared from partially methylated Hexamethyl-p-Terphenyl Polybenzimidazolium (HMT-PMBI) polymer, which was synthesized according to a reported route [18,35,36]. The process resulted in a membrane with a thickness of 81 ± 3 μm.

According to Burheim et al. the thermal conductivity of a Nafion® 115 membrane increased slightly when wet [19]. To ascertain if this effect holds true for the AEM investigated in this work, thermal conductivity measurements of this membrane were taken for two different humidifications. Dry samples were obtained by leaving them in a desiccator over night, achieving a relative humidity (RH) of 0%. Wet samples were humidified in deionized water at room temperature for more than 24 h after which they were expected to have reached 100% RH at room temperature. The humidification resulted in a water uptake corresponding to a λ-value of around 12 water molecules per ion exchange site, determined by weighing the samples in dry and wet condition. That is a reasonably high value compared to water uptake measurements of a similar membrane at 60 °C that reached a λ-value of around 12 at 95% RH [18]. The humidification procedure at room temperature was chosen to obtain a preliminary indication as to how the thermal conductivity depends on relative humidity without changing the experimental setup to suit a higher sample temperature.

After the desired humidification was achieved samples of 21 mm in diameter were punched out with a circular punch. This had to happen after humidification as the membrane is showing non-neglectable swelling when wetted. Thus, samples of 21 mm diameter with high RH contain less polymeric membrane material than the dry ones. The three-dimensional swelling of the membrane material is dependent on the temperature and the RH of the material. At 60 °C the in-plane swelling will reach 40% at RH = 100% and the volume swelling will reach more than 80% at RH = 100% [37].
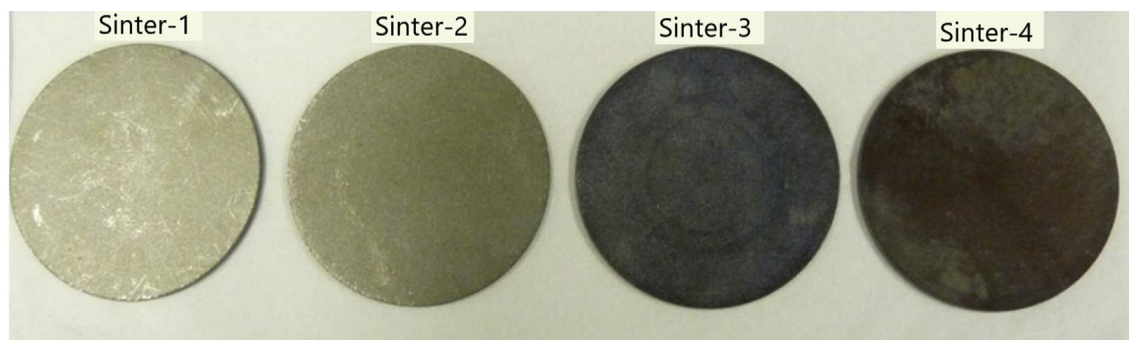

Fig. 2 — **Photograph of the four PTL materials with different surface treatments. From left to right: no treatment, oxalic acid, Pt coating A, Pt coating B [34].**
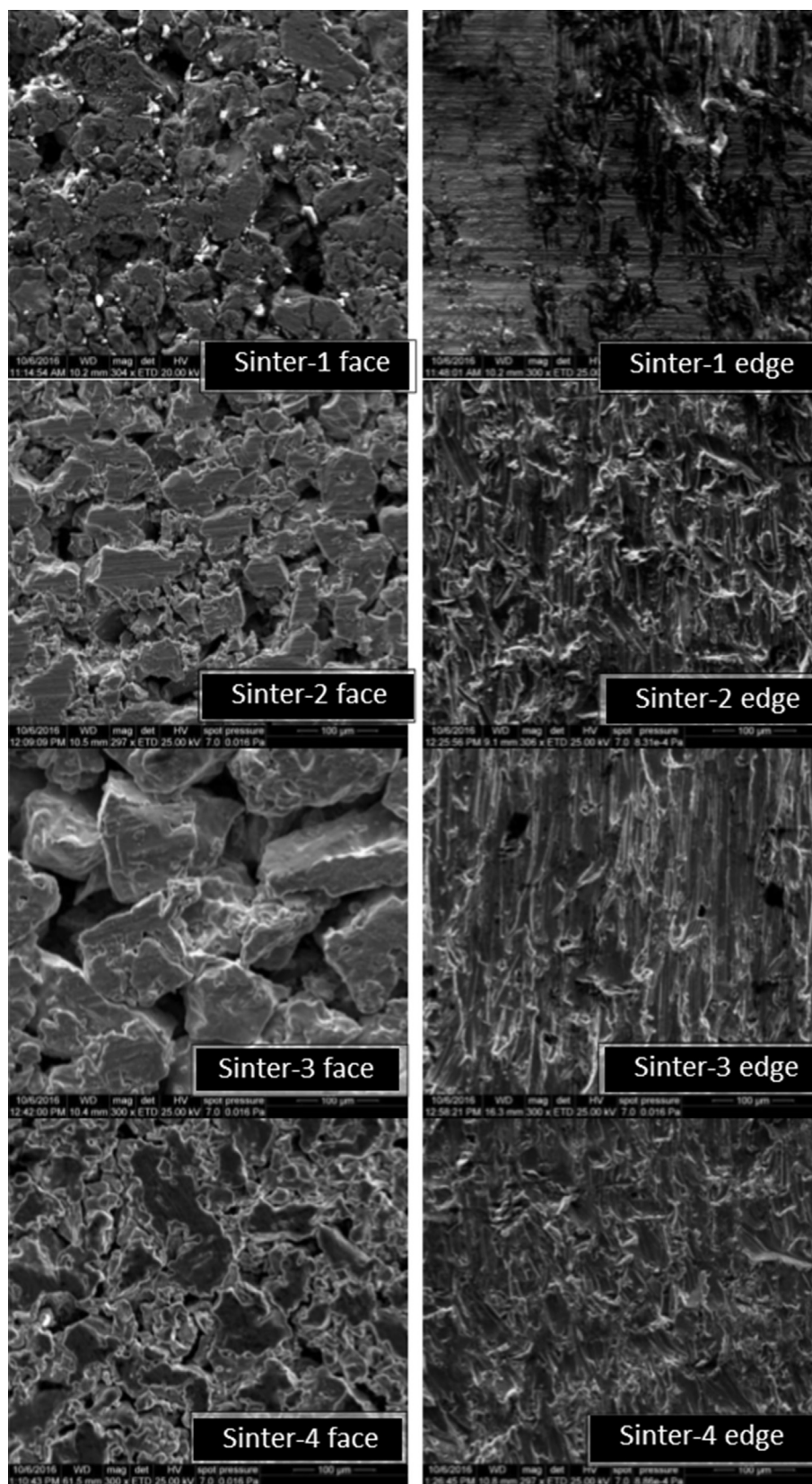
Fig. 3 — SEM graphs of the four PTL materials showing their differences in surface roughness and porosity. Sinter-3 shows larger particles on the face area than the other three materials [34].

Table 2 — Sinter materials porosity values with pore radii, all measured by mercury (Hg) intrusion.

Material	Porosity	Average pore radius	Median pore radius
Sinter-1	30.3%	3.8 μm	5.3 μm
Sinter-2	30.7%	2.3 μm	4.5 μm
Sinter-3	30.7%	6.2 μm	10.7 μm
Sinter-4	30.2%	1.0 μm	4.2 μm

To reduce the risk of a change in RH during measurements, the sample holding area was wrapped with parafilm for wet samples and only three different compaction pressures (5, 10 and 15 bar) were applied, so that the measurements required less time.

Thermal conductivity

A custom-built thermal conductivity measurement rig depicted in Fig. 4 was employed to measure the thermal conductivity of the materials used in an electrolyzer. Its ex-situ measurements are highly accurate [38]. A constant heat flux generated by thermoelectric Peltier modules on either side is applied to the sample through a cylindrical geometry that is symmetrical on top and bottom. Thermocouples 1—3 and 6—8 measure the temperature difference for a known distance and thermal conductivity of the steel. Thus, they measure the constant heat flux through the cylinders. These are thermally insulated by a custom-made heat jacket to prevent heat losses in the radial direction. Sample thickness can be recorded by 2 μm. A pneumatic setup can apply compaction pressures of up to 23 bar progressively under testing.
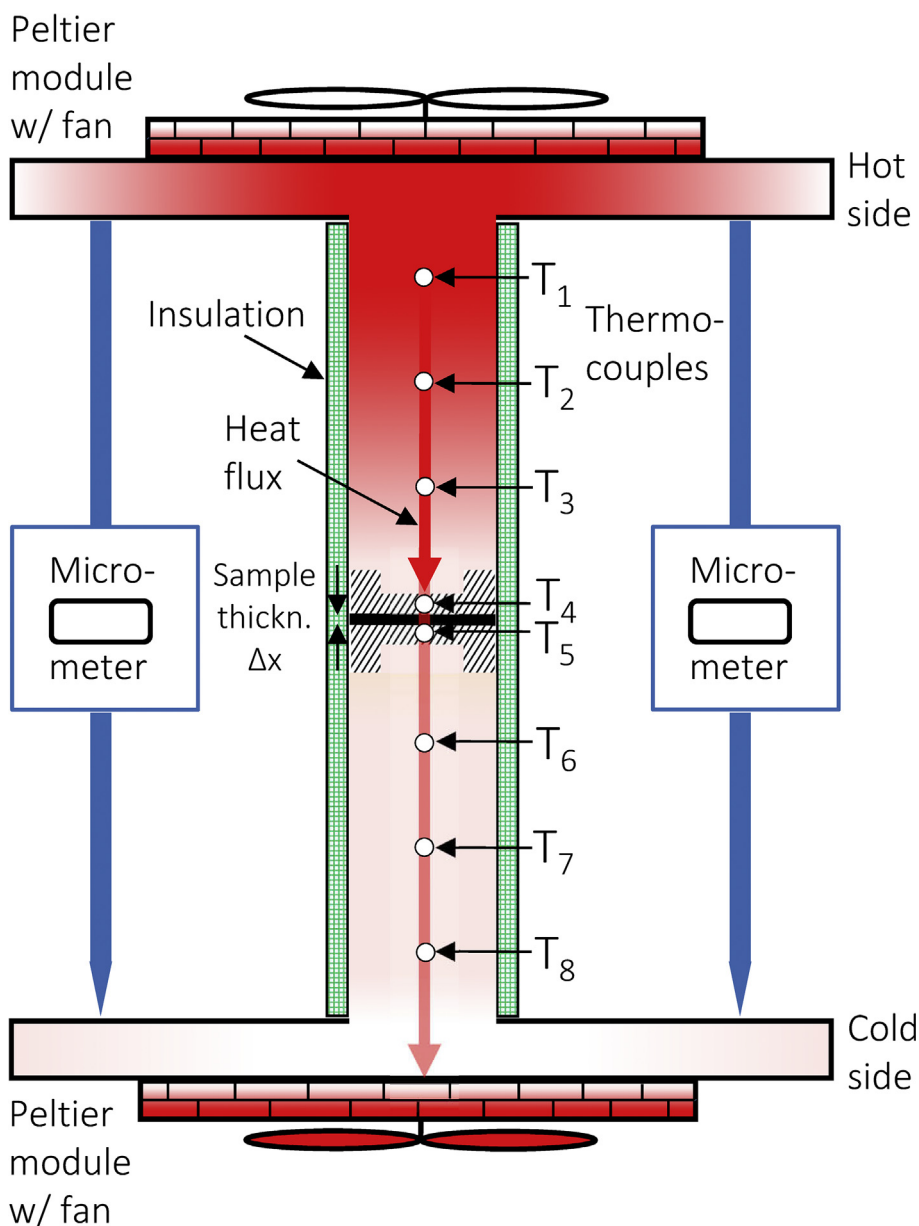

Fig. 4 — Sketch of the measurement rig.

Thermal resistance over the sample is measured by thermocouples 4 and 5 and recorded for different sample thicknesses, either by adequate sample supply or by stacking samples. The change in thermal resistance with thickness is then the inverse of thermal conductivity. This effectively decouples the bulk thermal resistance from the contact resistance between sample and apparatus. For a detailed description of how the setup works, we refer to our recent previous work, [38].

Modeling

The heat flow inside an electrolyzer was modeled with COMSOL Multiphysics. Heat is produced due to the electrical
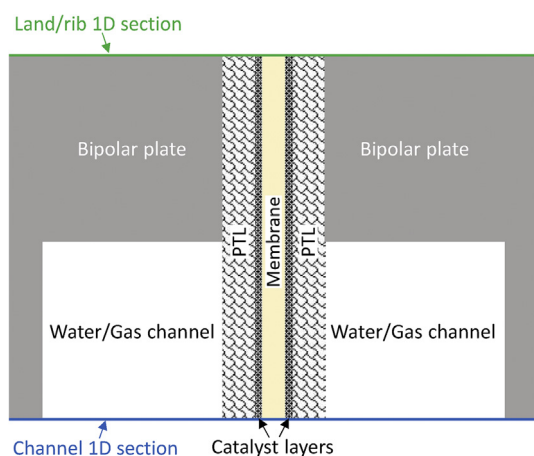

Fig. 5 – Electrolyzer geometry; coloured sections show where temperature distributions are evaluated in COMSOL. (For interpretation of the references to color in this figure legend, the reader is referred to the Web version of this article).

resistance in the ion exchange membrane and the electrodes. Some of that heat is needed in the endothermic water splitting reaction on the anode side. The geometry of the modeled part of the MEA is shown in Fig. 5.

The modeling area is a section of a larger electrolyzer and is symmetrically cut from it. The thermal conductivities of different materials used in the model are summarized in Table 3. Carbon fiber based fuel cell gas diffusion layers' thermal conductivities differ from the in-plane to the through-plane direction by a factor of 10 [39,40]. All the materials used in this study are isotropic in their thermal conductivity, hence the in-plane values are equal to the through-plane values.

The wet thermal conductivity of PTL material Sinter-2 was measured and is 4.3 times the dry value for the same material. Since only the Sinter-2 PTL was measured for thermal conductivity when wet, the other PTL materials' wet thermal conductivities were estimated using the same amplification factor as occurred for the wet Sinter-2 PTL. Thermal conductivity is changed significantly by the presence of liquid water. Therefore, also the catalyst layers have different thermal conductivity values when dry and when wet. In accordance with several studies on the matter, the value for the wet catalyst layers was set to three times the dry value [20,44,45].

Two heat transfer mechanisms are modeled in the channel; diffusion, and close to the walls, convection. For that a 50 μm boundary layer is defined where convective heat transfer is applied. The thermal conductivity values listed in Table 3 are values at 10 bar compaction pressure and are applied in the model. No current data was found on the actual compaction pressure in an electrolyzer, so 10 bar was chosen as an appropriate value. In the actual cell the compaction pressure will vary on the PTL due to the ribs from the flow field. Because of the stiff nature of the PTL here, as opposed to soft, fibrous PEMFC PTLs, the pressure on the MEA itself will be quite uniform.

Table 3 – Thermal conductivities used in the developed model.				
Material	κ (through-plane) WK^{-1}m^{-1}	κ (in-plane) WK^{-1}m^{-1}	Thickness μm	Ref.
Bipolar plates, stainless steel	20	20		[41]
Water	0.6	0.6		[42]
Hydrogen	0.17	0.17		[42]
Titanium-based porous transport layers				
Sinter-1, dry	1.9	1.9	1500	[a]
Sinter-1, wet	8.2	8.2	1500	[+]
Sinter-2, dry	1.6	1.6	1500	[a]
Sinter-2, wet	6.9	6.9	1500	[a]
Sinter-3, dry	1.3	1.3	1500	[a]
Sinter-3, wet	5.6	5.6	1500	[+]
Sinter-4, dry	1.9	1.9	1500	[a]
Sinter-4, wet	8.2	8.2	1500	[+]
Anode CL, wet	0.54	0.54	10	[20,43–45]
Cathode CL, dry	0.18	0.18	20	[20,43]
Cathode CL, wet	0.54	0.54	20	[44,45]
HMT-PMBI-Cl$^-$ anion exchange membrane				
RH at 20 °C = 0% $\widehat{=}$ λ = 0	0.19	0.19	81	[a]
RH at 20 °C = 100% $\widehat{=}$ λ = 12	0.21	0.21	81	[a]
Proton exchange membrane Nafion® 115				
RH at 20 °C = 100% $\widehat{=}$ λ = 22	0.25	0.25	127	[19]
[a] Values measured in this work at 10 bar compaction pressure; +values estimated based on measurements in this work.				

The heat distribution model was used to reveal the influence of different thermal conductivity values for PTL and membrane on the temperature distribution during operation of an electrolyzer. The setup was used for the PEMWE where PTLs were varied and for the AEMWE with the new membrane type with different RHs. Due to the lack of information in literature about alkaline electrolyzer catalyst materials, thermal conductivity values from PEM fuel cells were applied in the same manner as for the PEMWE. The model was also used to show the influence that different heat source mechanisms have on the overall temperature distribution. Three cases were considered, see Fig. 6 for a comparison of the three different setups.

Case 1. *(Hgas)* The channels on the anode (oxygen) side were filled with water while the channels on the cathode side contained only the produced hydrogen gas, see Fig. 6a. The entropic heat of the formation and evaporation of hydrogen was applied there, resulting in a heat sink on the cathode. On the anode side the produced oxygen is assumed to dissolve in the water at once, hence its entropic heat is assumed to be zero.

Case 2. *(Hdiss)* Water was assumed to be present in the channels on both sides of the MEA. On the cathode side, the produced hydrogen was assumed to dissolve in water immediately, resulting in the lack of entropic heat for the

evaporation of hydrogen. This assumption transformed the heat sink on the cathode side into a heat source, see Fig. 6b.

Case 3. *(HgasWevap)* Water was considered in the anode channels while hydrogen gas was assumed in the cathode channels. The entropic heat of hydrogen was considered as in Case 1 (Hgas). Additionally, ionic transport of water through the membrane was considered. 1.2 water molecules are transported (dragged) along with each anion and these water molecules were assumed to evaporate instantly when they reached the cathode side, resulting in an even greater heat sink than in Case 2 (Hdiss), see Fig. 6c.

A current density of 30 kAm^{-2} was applied for all PEMWE cases, a value that is claimed state of the art by commercial water electrolyzer producers, whilst 20 kA/m^{-2} was used for AWE. The latter is not common as of yet, but will be achieved once the AEM is used in commercial AEMWEs. It was recently demonstrated with alkaline water electrolysis using a very thin electrolyte layer [46]. The coolant temperature flowing through the BPPs on the left and right edge is maintained at 80 °C. The boundaries where another cell would adjoin were modeled as adiabatic. The electrical resistance of the PTLs is very small, its heat source contribution was therefore neglected [4]. Heat sources/sinks were implemented in the catalyst layers where the electrochemical reactions take place and in the membrane where ohmic resistance produces
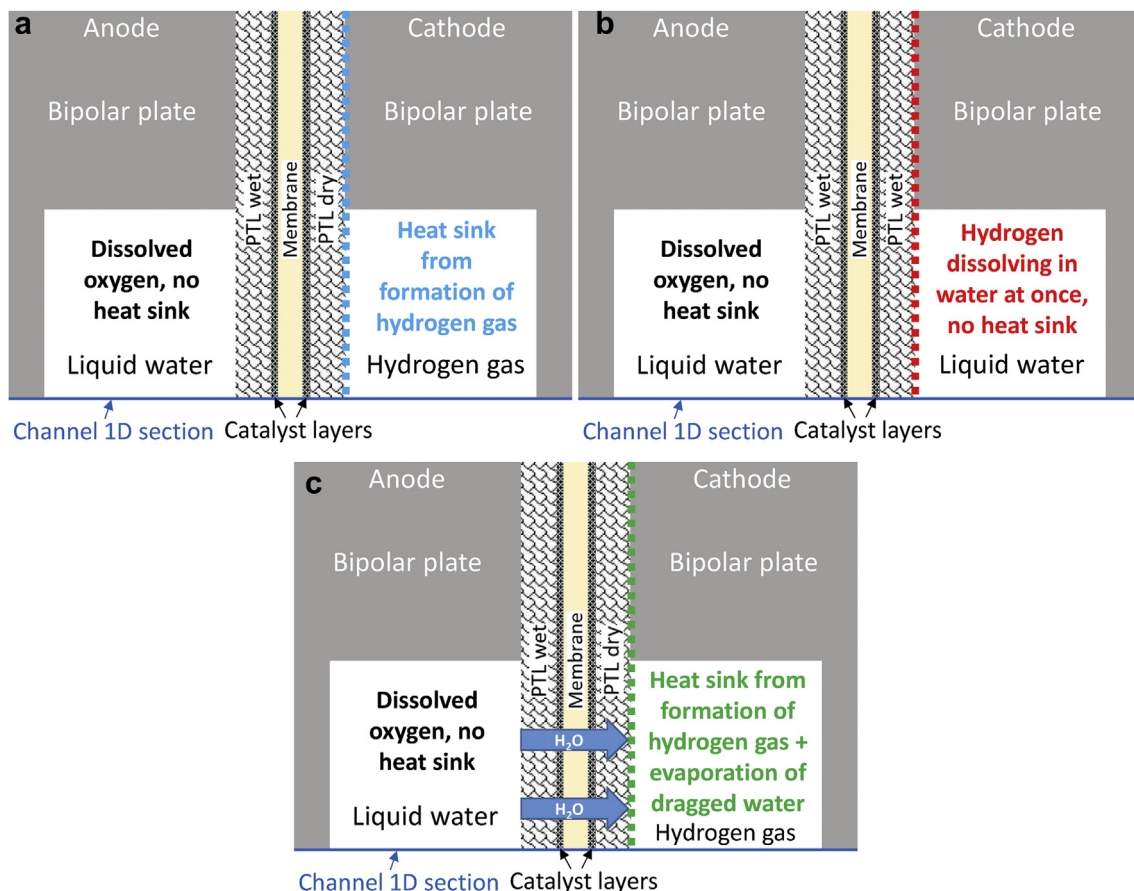

Fig. 6 – Setup for the different heat modeling cases.

considerable heat at the chosen current density. An overview of the implemented heat sources and sinks is provided in Table 4.

To model the ohmic heating in the membrane electrical conductivity values of 8.7 Sm⁻¹ for the PEM and 1 Sm⁻¹ for the (wet) AEM were used [47,52]. The ohmic heat for a dry AEM ($\lambda = 0$) would be extremely high, as the electrical conductivity is drastically lower by at least one order of magnitude [54]. This was not considered a likely scenario and is therefore not included in the modeling. The heat from activation losses was implemented according to the Tafel overpotential as functions of current density (denoted Tafel heat). They were found in Refs. [48,49] for PEMWE and in Ref. [53] for AWE. As mentioned, the entropic heat on the anode side is neglected. We assume instant dissolution of the oxygen in the water there, so that no heat is consumed to vaporize the produced oxygen. On the cathode side the entropic heat is included for cases 1 (Hgas) and 3 (HgasWevap). The entropy of the hydrogen half cell reaction is a topic that is still vividly discussed. Measurements report it to be close to zero [55] for an alkaline fuel cell, in the order of $-66\,\mathrm{Jk^{-1}molH_2^{-1}}$ [50] for a PEM

fuel cell and $87.6\,\mathrm{Jk^{-1}molH_2^{-1}}$ [56] by calorimetric experiments on a $Fe(CN)_6^{3-}/Fe(CN)_6^{4-}$ system. The value from Kjelstrup et al. was explicitly reported for open circuit potential. However, when a current is applied to the system, the hydrogen entropy seems to decrease while the entropy on the oxygen side increases. This could explain the wide range of reported values in the literature. Therefore we assume a distribution of the entropic heat between anode and cathode of 50/50. That means, since the entropic heat of oxygen formation is set to zero in all our cases, the entropic heat of hydrogen gas formation is $86.5\,\mathrm{Jk^{-1}mol\,H_2^1}$ (50% of $163\,\mathrm{Jk^{-1}mol\,H_2^1}$). 1 V in loss terms in Table 4 corresponds to 193 kJ/mol H_2.

Results and discussion

Thermal conductivity

The measured thermal conductivities for the PTLs and the AEM are presented in Table 5.

Table 4 — Heat sources used in the developed model.

Type	Location	Loss terms [V]	Current density j_{fc} [kAm⁻²]	Ref.	Heat flux at 80 °C q [Wm⁻²]
PEMWE					
for all cases					
Ohmic	Membrane	$j_{fc}/8.7\frac{S}{m}\cdot d_{memb}$*	30	[47]	13138
Tafel	Anode	$0.64 + 0.07\cdot log(j_{fc}/10000)$	30	[48,49]	21507
Tafel	Cathode	$0.01 + 0.03\cdot log(j_{fc}/10000)$	30	[48,49]	1289
Entropic	Anode	$0\cdot T/1000$	30		0
in addition					
for Case 1 (Hgas)					
Entropic	Cathode	$-0.44\cdot T/1000$	30	[50]	−4749
for Case 2 (Hdiss)				Σ Hgas	31185
Entropic	Cathode	$0\ T/1000$	30		0
for Case 3 (HgasWevap)				Σ Hdiss	35934
Entropic	Cathode	$-0.44\cdot T/1000$	30	[50]	−4749
Evaporation	Cathode	$-1.38\cdot T/1000$	30		−14582
				Σ HgasWevap	16603
AEMWE					
for Case 1 (Hgas)					
Ohmic	Membrane	$j_{fc}/1\frac{S}{m}\cdot d_{memb}$*	20	[51,52]	32400
Tafel	Anode	$0.16 + 0.20\cdot log(j_{fc}/10000)$	20	[53]	5973
Tafel	Cathode	$0.20 + 0.065\cdot log(j_{fc}/10000)$	20	[53]	4901
Entropic	Anode	$0\cdot T/1000$	20		0
Entropic	Cathode	$-0.44\cdot T/1000$	20	[50]	−3166
				Σ Hgas	40108

*d_{memb} according to Table 3.

Table 5 — Measured thermal conductivity values for the titanium-based PTLs and the anion exchange membrane at different relative humidities.

Compaction pressure [bar]	Titanium-based PTL					Anion exchange membrane	
	Sinter-1 κ [WK⁻¹m⁻¹]	Sinter-2 κ [WK⁻¹m⁻¹]	Sinter-2, wet κ [WK⁻¹m⁻¹]	Sinter-3 κ [WK⁻¹m⁻¹]	Sinter-4 κ [WK⁻¹m⁻¹]	RH = 0% κ [WK⁻¹m⁻¹]	RH = 100% κ [WK⁻¹m⁻¹]
5	1.6±0.2	1.4±0.2	7.2±1.8	1.2±0.3	1.7±0.4	0.17±0.06	0.20±0.03
10	1.9±0.3	1.6±0.2	6.9±1.6	1.3±0.2	1.9±0.2	0.19±0.04	0.21±0.03
15	2.2±0.2	1.9±0.2	7.1±1.8	1.5±0.2	2.2±0.3	0.19±0.05	0.23±0.03

The platinum-based PTLs show thermal conductivities between 1.2 and 2.2 $WK^{-1}m^{-1}$. For all PTL materials the thermal conductivity increases with increasing compaction pressure. That is somewhat surprising as the materials seem very stiff and showed minimal compaction when under pressure. The Sinter-3 material with pore radii about twice as large as the other materials has the lowest thermal conductivity of the four PTL materials. In connection with the pore radii the Sinter-3 material also has the roughest surface which makes for fewer contact points as indicated in Fig. 3. The effect of low overall thermal conductivity must be seen as a combination of those two factors. The influence of the surface properties on the overall thermal conductivity is further substantiated by the thermal conductivity value of Sinter-2, which has similar pore properties than Sinter-1 and Sinter-4 but has been surface-treated with oxalic acid, which seems to lessen the sinter material's ability to conduct heat at the surface when compared to the untreated Sinter-1 and the Pt-coated Sinter-4 materials.

The anion exchange membrane has a thermal conductivity between 0.17 and 0.23 $WK^{-1}m^{-1}$. Thermal conductivity is slightly higher for high compaction pressures here as well, the material showed compactions of maximum 2%, which is very low. The humidified sample with a λ-value of around 12 has an increased thermal conductivity. As mentioned these wetted samples contain less membrane material in the same sample size due to dimensional swelling. This seems to create better pathways for thermal transport inside the material. The increase in thermal conductivity fits results from the literature for Nafion® 115 membrane remarkably well. A thermal conductivity of 0.19 $WK^{-1}m^{-1}$ at $\lambda = 3$ and 0.22 $WK^{-1}m^{-1}$ at $\lambda = 11$ were reported at 9.3 bar compaction pressure [19]. In that study Nafion® 115 is also wetted to $\lambda = 22$ which yielded a thermal conductivity of 0.25 $WK^{-1}m^{-1}$ at 9.3 bar compaction pressure. This value is an indication then of how the thermal conductivity of the AEM may change at a similar water uptake level.

Thermal conductivity is plotted as a function of compaction pressure in Fig. 7 for the titanium-based PTLs and in Fig. 8 for the AEM.

Modeling

When comparing PEMWE and AEMWE heat sources, AEMWE produces significantly more heat for the same case. This is mainly due to the ohmic heating in the membrane being much larger for AEMWE due to lower ionic conductivity than for PEMWE. The Tafel heats are almost equally as large when seen combined, however, their distribution is vastly different, with the anode Tafel heat dominating for the PEMWE, while in AEMWE the anode Tafel heat is only slightly larger than for the cathode.

PEM water electrolysis

The model was solved with COMSOL and yielded a two-dimensional heat distribution for the described geometry, as shown in Fig. 9, exemplary for PEMWE Case 1 (Hgas) with Sinter-3 as PTL material. As the BPPs have a one to two orders of magnitude higher thermal conductivity than the channel media, they stay overall cooler during operation. This results in a slightly lower membrane temperature under the ribs of the flow field. There is an asymmetry to the heat distribution with more heat on the anode side of the cell. This is due to the large heat source on the anode from the Tafel heat of the OER.
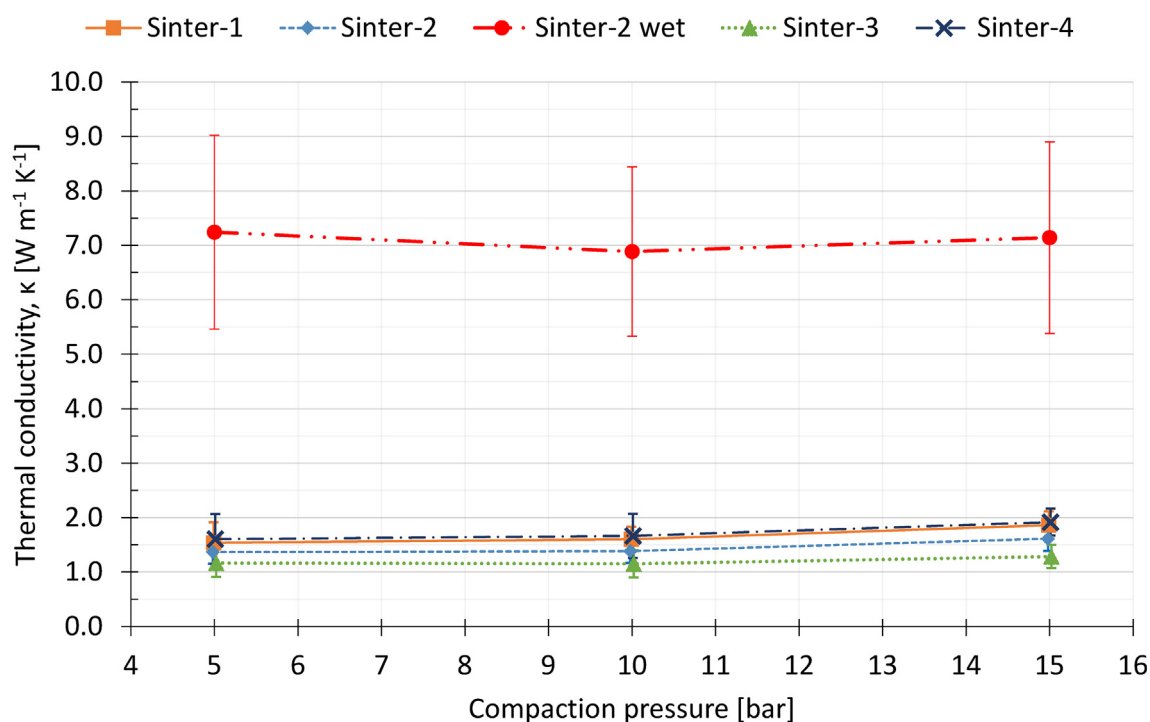

Fig. 7 – Measured thermal conductivities as a function of compaction pressure for the titanium-based PTLs in dry condition and the result from the wet measurement for PTL Sinter-2.
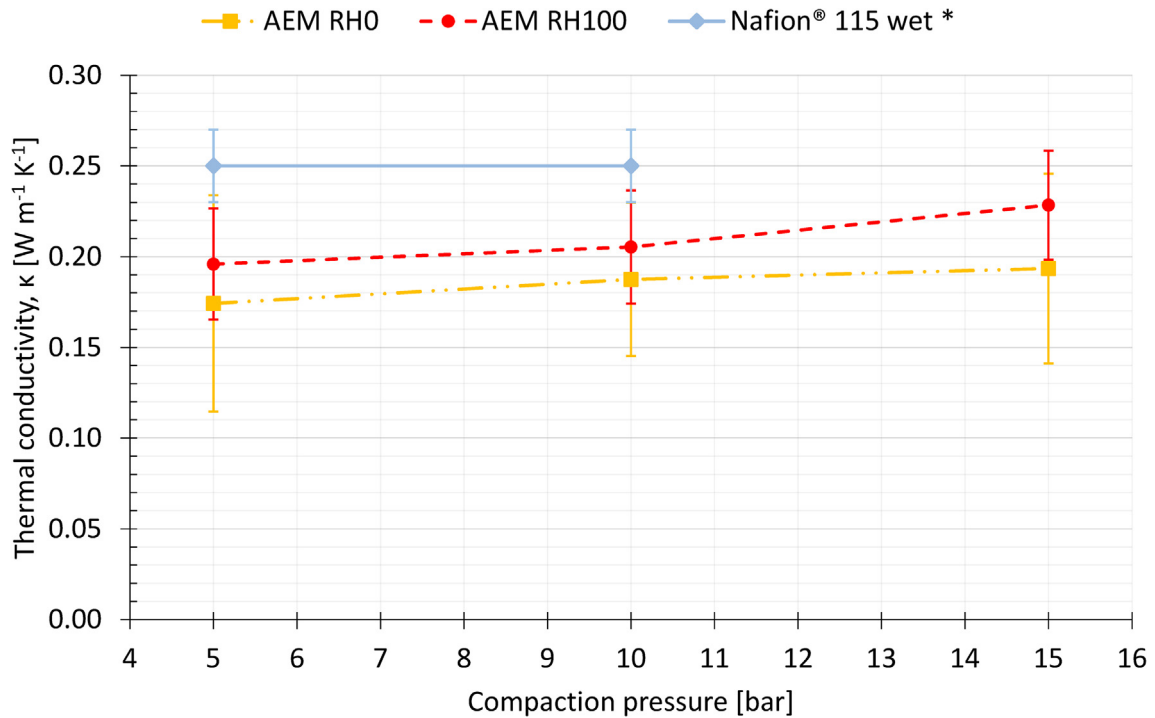
Fig. 8 – Measured thermal conductivities as a function of compaction pressure for the AEM and literature values (*) for a Nafion® 115 membrane [19].
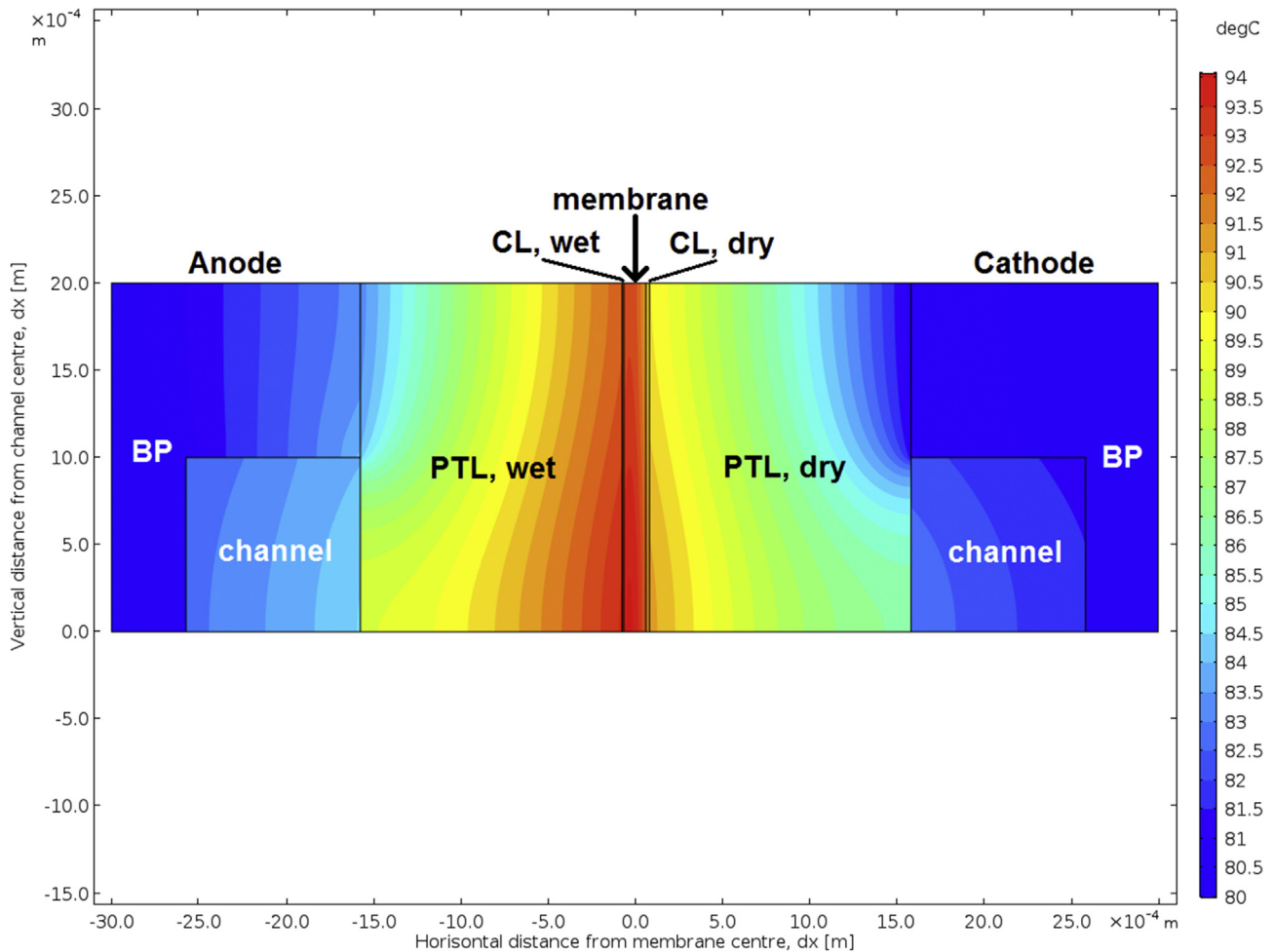

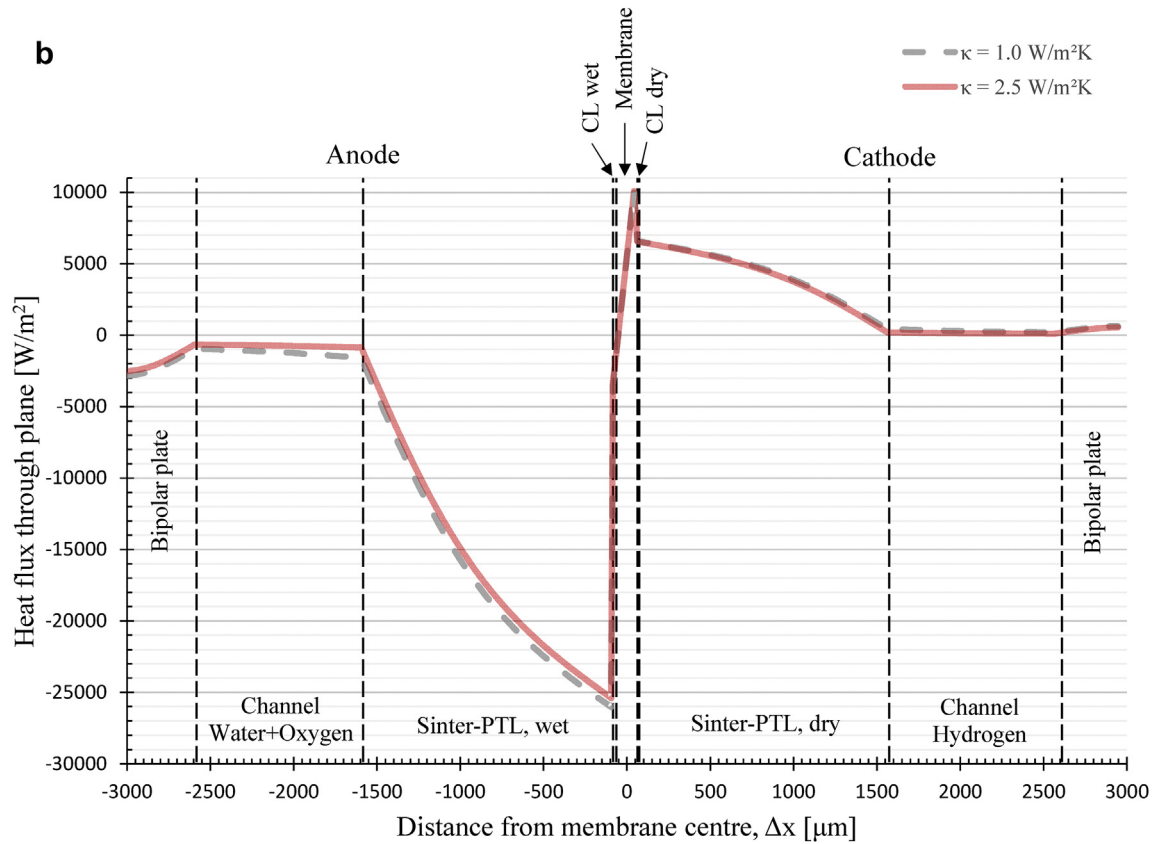**Fig. 9 –** Temperature contour plot of Case 1 (Hgas, Fig. 6a) for Sinter-3 PTL material.
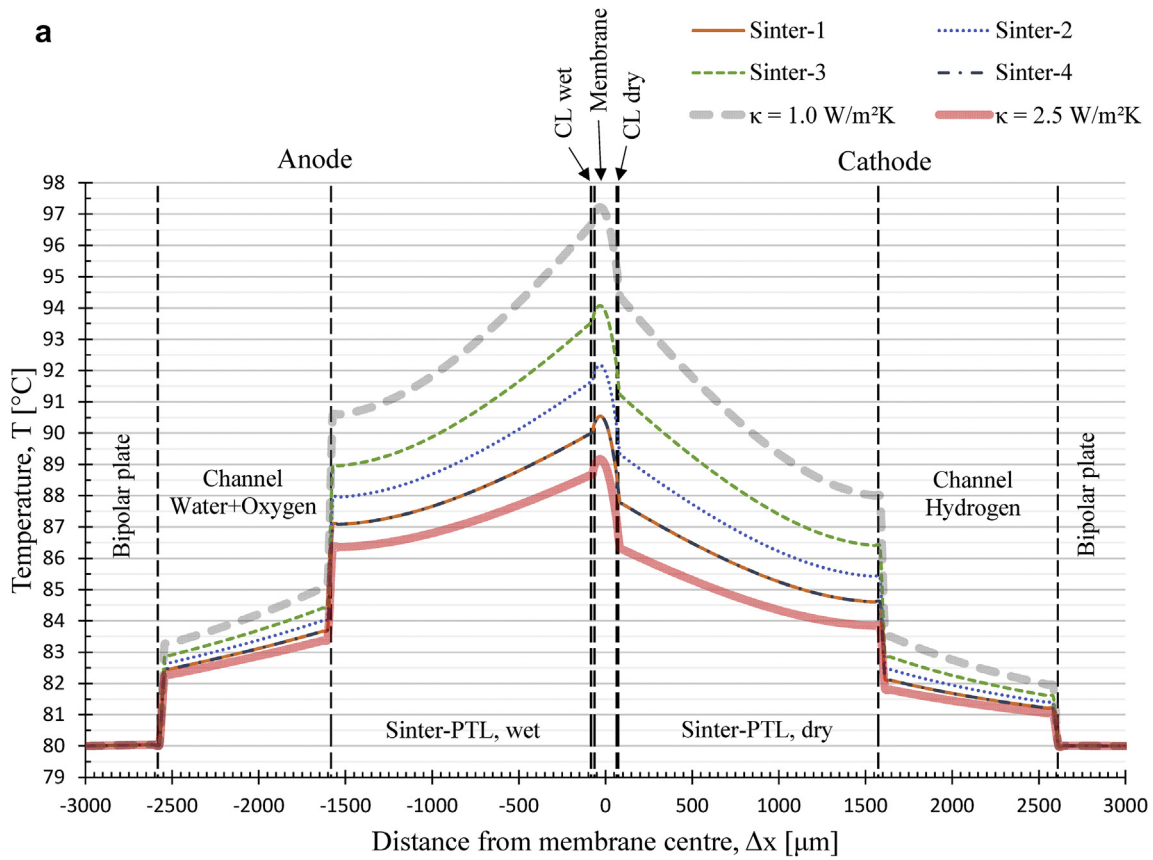
Fig. 10 – PEMWE profiles according to Case 1 (Hgas). Water on anode, hydrogen gas on cathode side. No entropic heat contribution on anode side. Dotted vertical lines represent interfaces between different materials.
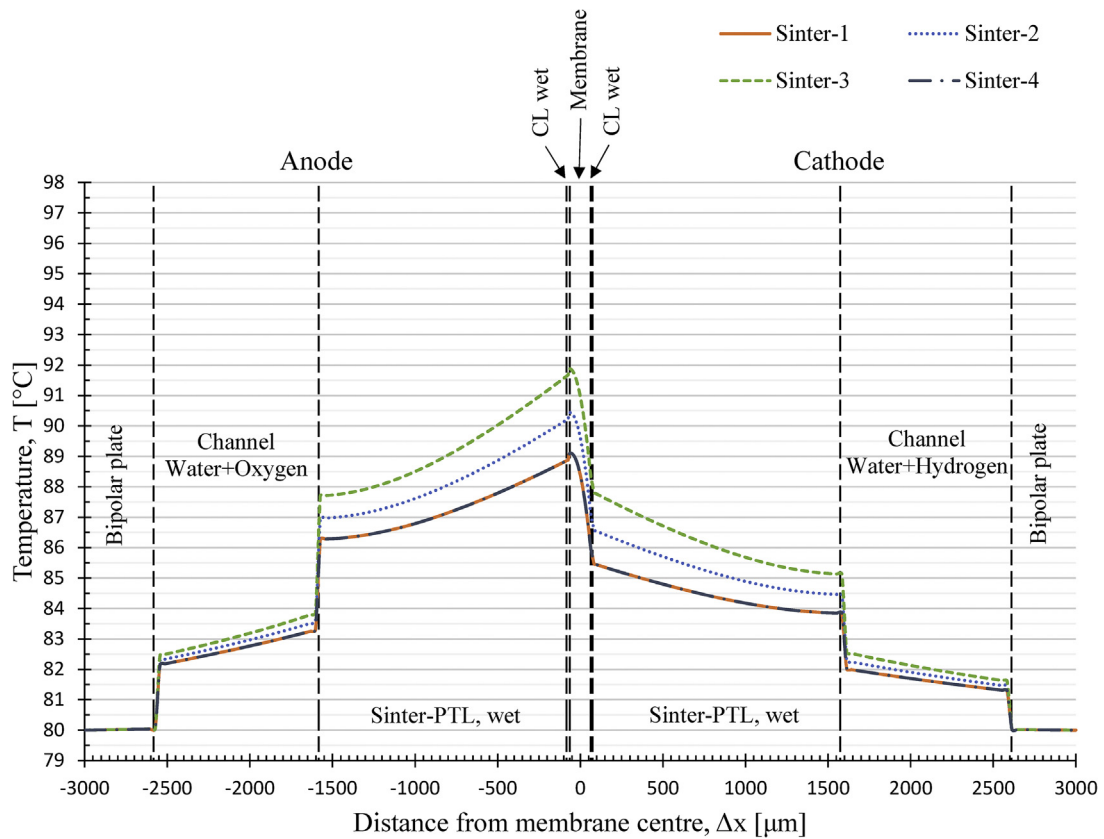
Fig. 11 – PEMWE channel temperature profile for Case 2 (Hdiss). No entropic heat contribution on cathode or anode side. Dotted vertical lines represent interfaces between different materials.
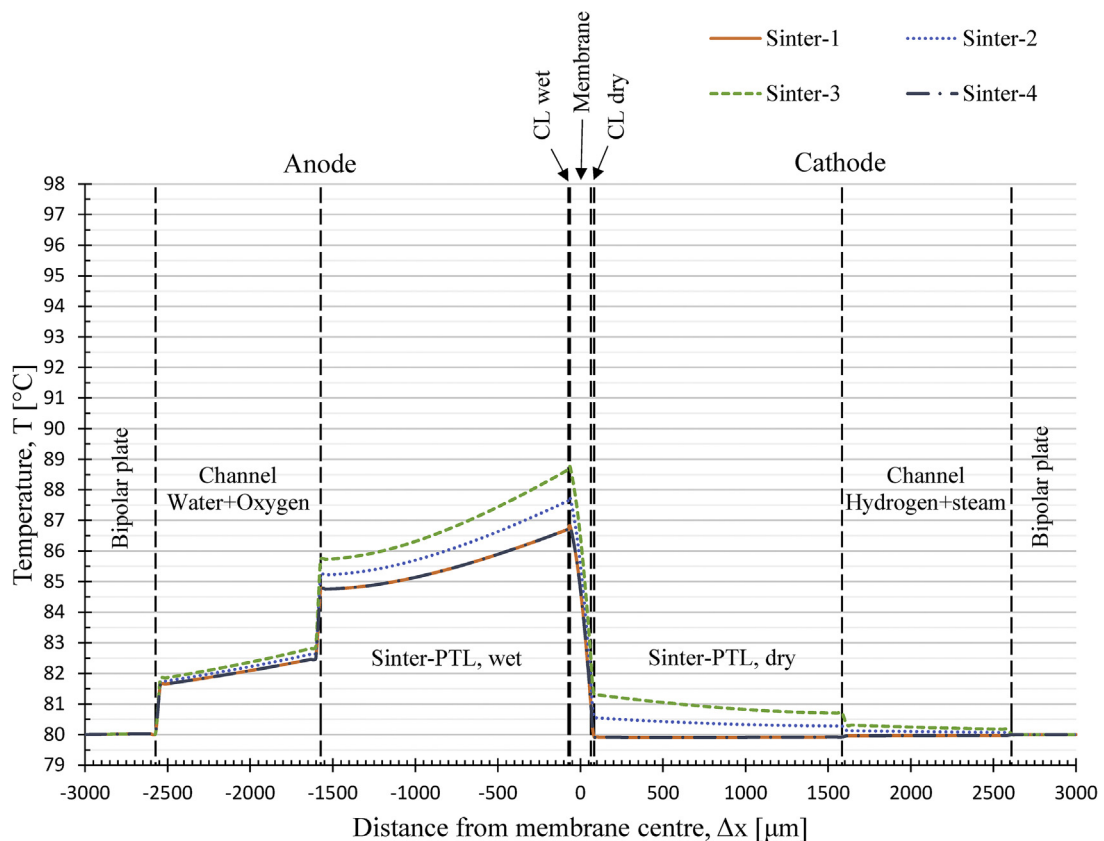

Fig. 12 – PEM WE channel temperature profile with water evaporation of water crossover for Case 3 (HgasWevap). No entropic heat contribution on anode side. Dotted vertical lines represent interfaces between different materials.

Additionally, the model neglects the entropic heat of the oxygen side but does include it for the hydrogen side, which results in a heat sink on the cathode. Furthermore, the overall higher thermal conductivities on the wet anode side cause a larger portion of the produced heat to be transported out via the anode to the BPP.

The plots in Figs. 10a, 11 and 12 and 13 illustrate the temperature profiles through the MEA in a straight line where there is a channel in the BPPs.

The non-linearity of the temperature gradients in Fig. 10a is due to the heat flux neither being uniform nor isotropic, as seen in Fig. 10b. Since the model is two-dimensional, heat will diffuse in two dimensions as well, as seen in Fig. 9. This leads to the non-linear temperature distribution. The difference in thermal conductivity for the four Sinter-PTLs results in a 3.5 K difference in maximum temperature in the membrane close to the anode catalyst layer. These maximum temperatures are rather high for the Nafion® membrane to perform as intended over prolonged periods of time, it being based on water which will evaporate quickly at these temperatures. In addition to the four tested PTLs, results for thermal conductivity values of 1.0 and 2.5 $WK^{-1}m^{-1}$ for the PTLs were added to show the suspected range of materials used as PTL. The maximum temperature shows a considerable 17 K between BPP and membrane.

In Fig. 10b the heat flux for Case 1 (Hgas) is depicted for the two thermal conductivity values of 1.0 and 2.5 $WK^{-1}m^{-1}$ from

Fig. 10a. Negative heat flux values flow towards the anode side, positive values towards the cathode side. The maximum heat flux inside the membrane is above 25 kWm^{-2}, for both thermal conductivity values considered. Such a high heat flux will drag water with it in addition to the ionic water drag effect. As the heat flux is positive from the anode catalyst layer to the cathode catalyst layer, it will flow towards the cathode and hence drag water from the water-filled anode channel through the membrane towards the hydrogen gas-filled cathode channel. That might save the membrane from drying out despite the high temperatures. The highest heat flux is shown in the catalyst layers. This is due to a large portion of the heat being created by ohmic resistance in the membrane. Especially the anode CL experiences an enormous heat flux. That means, that even small changes of its thermal conductivity will have a large impact on the heat distribution in the cell.

Fig. 11 shows the temperature profile in the channel for Case 2 (Hdiss).

Despite the lack of a heat sink, temperatures are slightly lower than for Case 1 (Hgas) for all four Sinter PTL materials. The difference between Sinter-3 and Sinter-1/4 maximum temperature is around 3 K, with a maximum temeprature difference from BPP to membrane of 12 K.

Fig. 12 shows the temperature profile in the channel for Case 3 (HgasWevap).

In Case 3 (HgasWevap) two factors contribute to the heat sink in the cathode catalyst layer, the entropic heat of
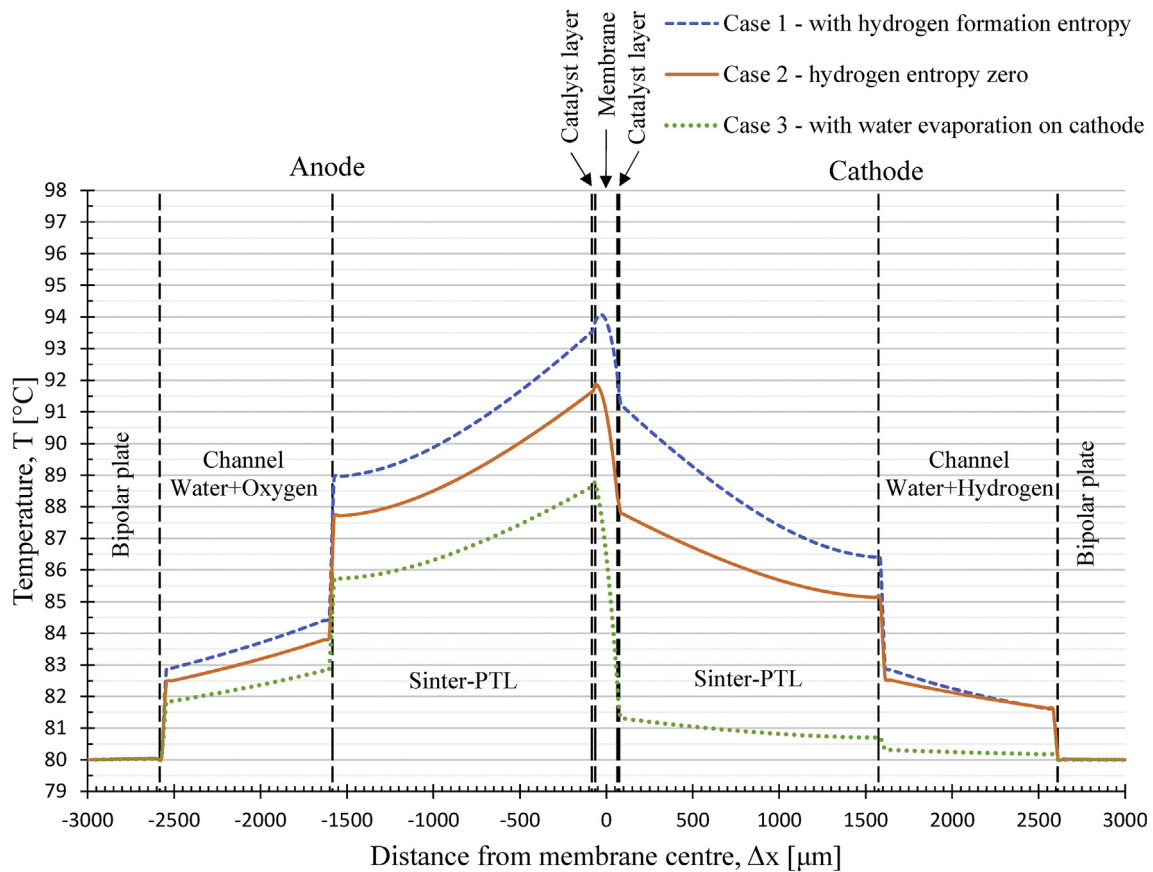

Fig. 13 – PEMWE channel temperature profile with different heat sources on cathode side. Dotted vertical lines represent interfaces between different materials.
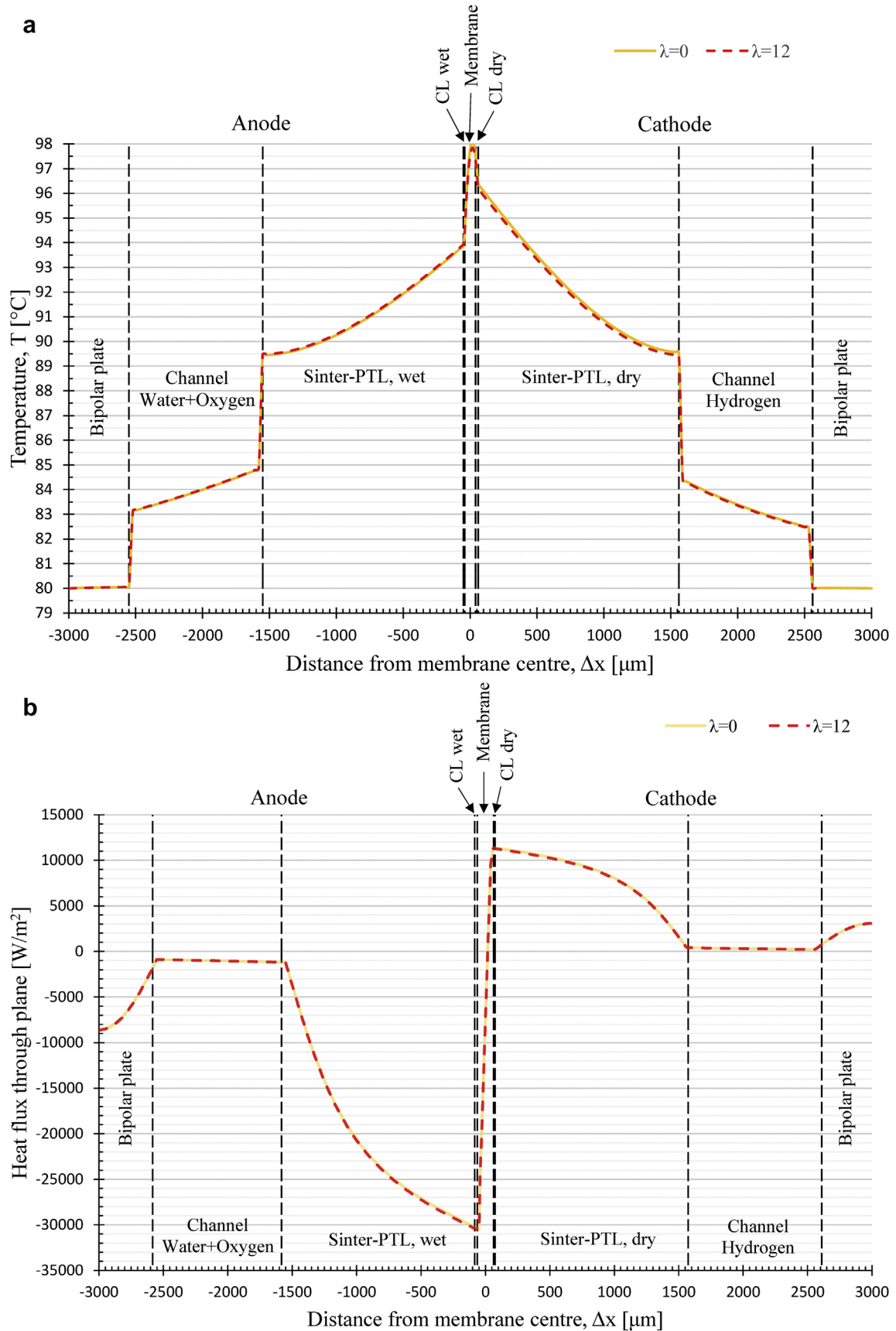
Fig. 14 – **AEMWE profiles according to Case 1 (Hgas). Water on anode, hydrogen gas on cathode side. Dotted vertical lines represent interfaces between different materials.**

formation of hydrogen and the evaporation entropy of the water dragged along by ions crossing the membrane. This results in overall lower temperatures, also in the membrane. The temperature distributions are grouped closer together, none of the materials produces temperatures above 90 °C in the membrane. Due to the large heat sink the temperature distribution is very asymmetric, with cooling channel temperatures in all materials from the CL outwards on the cathode side. The maximum temperature difference of around 9 K is then observed from the anode BPP to the membrane.

Fig. 13 compares the temperature profiles for all three cases for the Sinter-3 material, which showed the highest temperatures in the different cases.

The difference in maximum temperature in the membrane is about 5 K for the three cases. This difference depends solely on the modeling of entropic heat on the cathode side. Case 1 (Hgas) poses the highest temperature. Even though it considers the heat sink of forming hydrogen gas, the lower thermal conductivities in dry CL and PTL cause a build-up of temperature. Case 2 (Hdiss) without heat sink due to the assumption that hydrogen will dissolve in the water instantly, is modeled to a 2 K lower maximum temperature. This may be surprising, given that the heat sources are largest for this case, but liquid water is assumed in both channels, resulting in significantly higher thermal conductivities in CL and PTL on the cathode side than for Case 1 (Hgas), which means a higher cathode heat flux that reduces the maximum membrane temperature compared to Case 1 (Hgas). Case 3 (HgasWevap) considers a significant heat sink on the cathode due to the evaporation of the water transported along with the anions, therefore it poses the lowest temperature throughout the MEA.

When considering a real PEMWE, it is safe to assume that some water will evaporate in the cathode catalyst layer and thus cool it down. However, some of the water might accumulate in liquid form and get reabsorbed into the membrane. We expect the heat distribution in an actual electrolyzer to lie somewhere between Case 1 (Hgas) and Case 3 (HgasWevap), which are the cases with hydrogen gas in the cathode channel. The important observation here is that when pursuing temperature gradient reduction, it is more important to consider liquid water than entropic heat. That is, increased thermal conductivity and increased cooling effect in the presence of liquid water in the PTL outnumbers the impact of the cooling term of the gasification of hydrogen. Additionally, liquid water has a benign effect on any unwanted consequences of thermal gradients, like mechanical stress and increased degradation rates.

AEM water electrolysis
Fig. 14 shows the temperature and heat flux profile for an electrolyzer with an anion exchange membrane with different relative humidities, differentiated by their respective water uptake values of $\lambda = 0$ for RH = 0 and $\lambda = 12$ for RH = 100. The setup is very similar to the PEM electrolyzer in the preceding section, only the membrane was exchanged to the thinner AEM that also has a slightly lower thermal conductivity than Nafion® 115. Additionally, different values from the literature for the Tafel heat had to be used, as the half cell reactions are different for AEMWE. For the heat production modeling Case 1

(Hgas) from the PEM section was chosen for best comparability. Thermal conductivity data was used from the PTL with the intermediate thermal conductivity, resulting in an intermediate membrane temperature.

The results show that the difference in membrane thermal conductivity due to humidifaction does not have a significant influence on the temperature distribution. These results are meant to illustrate that a locally dry membrane would not have an immediate effect on the temperature distribution. As mentioned however, a completely dried out membrane would result in enormous ohmic heating.

The maximum temperature is reached in the membrane and is very similar for the two cases of membrane humidity, topping out at around 98 °C. The AEM is significantly thinner than the PEM used in these simulations and has a better ion conductivity, this results in almost four times less ohmic heating in the membrane and thus a smaller contribution to the maximum temperature. Also for the AEM the highest heat fluxes will occur in the catalyst layers where the large amount of heat from the membrane has to pass through to be transported towards the cooling channels. This emphasizes the importance of knowing and manipulating the thermal conductivity of the CL itself, but also the adjoining PTL for a good heat management.

Conclusion

The temperature distribution in water electrolyzers was studied for the first time in literature. Thermal conductivity values for some key components were measured and reported for different compaction pressures and humidities. These were used in a 2D heat distribution model to analyze the temperature distribution through the MEA in a PEM and an AEM water electrolyzer.

The four different titanium-based Sinter-PTLs showed thermal conductivities between 1 and 2.5 $WK^{-1}m^{-1}$ when dry. They consist of the same material but have differing porosity properties and different surface treatments applied to them. Both Sinter-1 whicht was not surface-treated and the Sinter-4 treated with Pt-coating method B had the highest thermal conductivity of 1.9 $WK^{-1}m^{-1}$ at 10 bar compaction pressure. Their pore radii were comparable, as was their surface roughness. The Sinter-2 material treated with oxalic acid had a thermal conductivity of 1.6 $WK^{-1}m^{-1}$ and had similar pore and surface properties as Sinter-1 and Sinter-4. The Sinter-3 material treated with Pt-coating method A showed significantly higher pore radii and surface roughness, which resulted in the lowest thermal conductivity of the four PTLs, it was 1.3 $WK^{-1}m^{-1}$ at a compaction pressure of 10 bar. The Sinter-2 PTL material was also measured when wet, which resulted in an increase in thermal conductivity by a factor of more than four to 6.9 $WK^{-1}m^{-1}$. Modeling the heat distribution with these PTL values resulted in temperature differences from the center of the MEA to the BPP to reach 7–17 K, depending on the material and type of heat source modeling. These are considerable temperature gradients that need to be addressed, especially with respect to the longterm health of the water based membrane used in the PEM electrolyzer.

The anion exchange membrane showed thermal conductivities between 0.17 and 0.23 $WK^{-1}m^{-1}$ depending on relative humidity and compaction pressure. Heat distribution modeling showed a temperature difference of more than 18 K from the center of the MEA to the BPPs. The thermal conductivity of the AEM is slightly lower than for Nafion® 115, which was used for the PEM electrolyzer model. That makes it suitable contender for implementing a membrane in the alkaline electrolyzer technology. This technology enables the use of non-noble metals as electrodes, which provides a great cost advantage.

For the PEMWE, when using liquid water in the cathode flow channel with hydrogen gas, the maximum temperature changes from 94 °C to 92 °C, even though the entropic cooling from hydrogen gasification is removed, because of the increased thermal conductivities in CL and PTL due to the presence of liquid water.

In the future, more of the water electrolyzer-specific materials such as different PTLs, CLs and membranes should be classified in terms of thermal conductivity. This would enable even more precise heat distribution models that will ultimately improve performance of the next-generation water electrolyzer technology. To date, the temperature control is performed by controlling the temperature of the electrolyte. As shown in this work, however, this temperature may deviate considerably from the temperature in the core of the cell.

Acknowledgements

REFERENCES

[1] Bockris J, Appleby A. The hydrogen economy: an ultimate economy? Environ This Mon 1972;1(1):29—35.
[2] M. Carmo, D. L. Fritz, J. Mergel, D. Stolten, A comprehensive review on PEM water electrolysis, Int J Hydrogen Energy 38.
[3] I. Vincent, D. Bessarabov, Low cost hydrogen production by anion exchange membrane electrolysis: a review, Renew Sustain Energy Rev 81.
[4] Burheim OS. Engineering energy storage. 1st ed. Elsevier Academic Press; 2017.
[5] Hillestad M, Ostadi M, Serrano G, Rytter E, Austbø B, Pharoah JG, Burheim OS. Improving carbon efficiency and profitability of the biomass to liquid process with hydrogen from renewable power. Fuel 2018;234:1431—51.
[6] A. Buttler, H. Spliethoff, Current status of water electrolysis for energy storage, grid balancing and sector coupling via power-to-gas and power-to-liquids: a review, Renew Sustain Energy Rev 82.
[7] Bockris JO. The hydrogen economy: its history. Int J Hydrogen Energy 2013;38(6):2579—88.
[8] Gahleitner G. Hydrogen from renewable electricity: an international review of power-to-gas pilot plants for

[9] stationary applications. Int J Hydrogen Energy 2013;38(5):2039—61.
[9] Barthels H, Brocke W, Bonhoff K, Groehn H, Heuts G, Lennartz M, Mai H, Mergel J, Schmid L, Ritzenhoff P. Phoebus-Jülich: an autonomous energy supply system comprising photovoltaics, electrolytic hydrogen, fuel cell. Int J Hydrogen Energy 1998;23(4):295—301.
[10] Ulleberg Øystein, Nakken T, Eté A. The wind/hydrogen demonstration system at Utsira in Norway: evaluation of system performance using operational data and updated hydrogen energy system modeling tools. Int J Hydrogen Energy 2010;35(5):1841—52.
[11] Gutiérrez-Martín F, Guerrero-Hernández I. Balancing the grid loads by large scale integration of hydrogen technologies: the case of the Spanish power system. Int J Hydrogen Energy 2012;37(2):1151—61.
[12] Qadrdan M, Abeysekera M, Chaudry M, Wu J, Jenkins N. Role of power-to-gas in an integrated gas and electricity system in Great Britain. Int J Hydrogen Energy 2015;40(17):5763—75.
[13] Babic U, Suermann M, Büchi FN, Gubler L, Schmidt TJ. Critical review—identifying critical gaps for polymer electrolyte water electrolysis development. J Electrochem Soc 2017;164(4):F387—99.
[14] Godula-Jopek A, Millet P. Hydrogen production : by electrolysis, chap. 9. Berlin: John Wiley & Sons, Incorporated; 2015. p. 383—94.
[15] Schmidt O, Gambhir A, Staffell I, Hawkes A, Nelson J, Few S. Future cost and performance of water electrolysis: an expert elicitation study. Int J Hydrogen Energy 2017;42(52):30470—92.
[16] Rasten E, Hagen G, Tunold R. Electrocatalysis in water electrolysis with solid polymer electrolyte. Electrochim Acta 2003;48(25):3945—52.
[17] Tunold R, Marshall AT, Rasten E, Tsypkin M, Owe L-E, Sunde S. Materials for electrocatalysis of oxygen evolution process in PEM water electrolysis cells. ECS Trans 2010;25(23):103—17.
[18] Novitski D, Kosakian A, Weissbach T, Secanell M, Holdcroft S. Electrochemical reduction of dissolved oxygen in alkaline, solid polymer electrolyte films. J Am Chem Soc 2016;138(47):15465—72.
[19] Burheim O, Vie P, Pharoah J, Kjelstrup S. Ex situ measurements of through-plane thermal conductivities in a polymer electrolyte fuel cell. J Power Sources 2010;195(1):249—56.
[20] Burheim OS, Su H, Hauge HH, Pasupathi S, Pollet BG. Study of thermal conductivity of PEM fuel cell catalyst layers. Int J Hydrogen Energy 2014a;39(17):9397—408.
[21] Miles MH, Kissel G, Lu PWT, Srinivasan S. Effect of temperature on electrode kinetic parameters for hydrogen and oxygen evolution reactions on nickel electrodes in alkaline solutions. J Electrochem Soc 1976;123(3):332—6.
[22] Bailleux C. Advanced water alkaline electrolysis: a two-year running of a test plant. Int J Hydrogen Energy 1981;6(5):461—71.
[23] Stojić DL, Marčeta MP, Sovilj SP, Miljanić Śćepan S. Hydrogen generation from water electrolysis—possibilities of energy saving. J Power Sources 2003;118(1):315—9.
[24] Maeda T, Nagata Y, Endo N, Ishida M. Effect of water electrolysis temperature of hydrogen production system using direct coupling photovoltaic and water electrolyzer. J Int Counc Electr Eng 2016;6(1):78—83.
[25] Hug W, Bussmann H, Brinner A. Intermittent operation and operation modeling of an alkaline electrolyzer. Int J Hydrogen Energy 1993;18(12):973—7.
[26] Ulleberg Øystein. Modeling of advanced alkaline electrolyzers: a system simulation approach. Int J Hydrogen Energy 2003;28:21—33.
[27] Diéguez P, Ursúa A, Sanchis P, Sopena C, Guelbenzu E, Gandía L. Thermal performance of a commercial alkaline

water electrolyzer: experimental study and mathematical modeling. Int J Hydrogen Energy 2008;33(24):7338–54.

[28] Abdin Z, Webb C, Gray E. Modelling and simulation of an alkaline electrolyser cell. Energy 2017;138:316–31.

[29] Choi P, Bessarabov DG, Datta R. A simple model for solid polymer electrolyte (SPE) water electrolysis. Solid State Ionics 2004;175(1):535–9.

[30] Harrison K, Hernández-Pacheco E, Mann M, Salehfar H. Semiempirical model for determining PEM electrolyzer stack characteristics. J Fuel Cell Sci Technol 2005;3(2):220–3.

[31] Lebbal M, Lecœuche S. Identification and monitoring of a PEM electrolyser based on dynamical modelling. Int J Hydrogen Energy 2009;34(14):5992–9.

[32] Awasthi A, Scott K, Basu S. Dynamic modeling and simulation of a proton exchange membrane electrolyzer for hydrogen production. Int J Hydrogen Energy 2011;36:14779–86.

[33] Kaya MF, Demir N. Numerical investigation of PEM water electrolysis performance for different oxygen evolution electrocatalysts. Fuel Cells 2017;7(1):37–47.

[34] Serre G, Chandesris M, Fouda-Onana F, Brun-Buisson D, Skjetne P, Bergstrøm T, Bromberger K, Smolinka T, Ghinaiya J. MEGASTACK: D2.3 Functional and validated multi-scale and multi-phase models for PEMwater electrolyzer. Tech Rep CEA Tech 2016:14–41.

[35] Wright AG, Holdcroft S. Hydroxide-stable ionenes. ACS Macro Lett 2014;3(5):444–7.

[36] Wright AG, Fan J, Britton B, Weissbach T, Lee H-F, Kitching EA, Peckham TJ, Holdcroft S. Hexamethyl-p-terphenyl poly(benzimidazolium): a universal hydroxide-conducting polymer for energy conversion devices. Energy Environ Sci 2016;9:2130–42.

[37] Luo X, Wright A, Weissbach T, Holdcroft S. Water permeation through anion exchange membranes. J Power Sources 2018;375:442–51.

[38] R. Bock, A. D. Shum, X. Xiao, H. Karoliussen, F. Seland, I. V. Zenyuk, O. S. Burheim, Thermal conductivity and compaction of GDL-MPL interfacial composite material, J Electrochem Soc 165 (7).

[39] Sadeghi E, Djilali N, Bahrami M. A novel approach to determine the in-plane thermal conductivity of gas diffusion layers in proton exchange membrane fuel cells. J Power Sources 2011;196(7):3565–71.

[40] Teertstra P, Karimi G, Li X. Measurement of in-plane effective thermal conductivity in PEM fuel cell diffusion media. Electrochim Acta 2011;56(3):1670–5.

[41] R. Taherian, A review of composite and metallic bipolar plates in proton exchange membrane fuel cell: materials, fabrication, and material selection, J Power Sources 265.

[42] Rumble J, editor. CRC handbook of chemistry and physics. 98 edn. Taylor & Francis; 2017.

[43] Ahadi M, Tam M, Saha MS, Stumper J, Bahrami M. Thermal conductivity of catalyst layer of polymer electrolyte membrane fuel cells: Part 1 – experimental study. J Power Sources 2017;354:207–14. ISSN 0378-7753.

[44] Burheim OS, Aslan M, Atchison JS, Presser V. Thermal conductivity and temperature profiles in carbon electrodes for supercapacitors. J Power Sources 2014b;246:160–6.

[45] Burheim OS, Pharoah JG, Lampert H, Vie PJS, Kjelstrup S. Through-plane thermal conductivity of PEMFC porous transport layers. J Fuel Cell Sci Technol 2011;8(2):21013.

[46] Schalenbach M, Kasian O, Mayrhofer KJ. An alkaline water electrolyzer with nickel electrodes enables efficient high current density operation. Int J Hydrogen Energy 2018;43(27):11932–8.

[47] Burheim OS, Ellila G, Fairweather JD, Labouriau A, Kjelstrup S, Pharoah JG. Ageing and thermal conductivity of Porous Transport Layers used for PEM fuel cells. J Power Sources 2013a;221:356–65.

[48] Springer TE, Zawodzinski TA, Gottesfeld S. Polymer electrolyte fuel cell model. J Electrochem Soc 1991;138(8):2334–42.

[49] Rasten E. Electrocatalysis in water electrolysis with solid polymer electrolyte. Ph.D. thesis. NTNU; 2001.

[50] Kjelstrup S, Vie PJS, Akyalcin L, Zefaniya P, Pharoah JG, Burheim OS. The Seebeck coefficient and the Peltier effect in a polymer electrolyte membrane cell with two hydrogen electrodes. Electrochim Acta 2013;99:166–75.

[51] Burheim OS, Su H, Pasupathi S, Pharoah JG, Pollet BG. Thermal conductivity and temperature profiles of the micro porous layers used for the polymer electrolyte membrane fuel cell. Int J Hydrogen Energy 2013b;38(20):8437–47.

[52] Thomas OD, Soo KJWY, Peckham TJ, Kulkarni MP, Holdcroft S. A stable hydroxide-conducting polymer. J Am Chem Soc 2018;134:10753–6.

[53] Divisek J. Water electrolysis in low- and medium temperature regime, chap. Chapter 2. New York: Elsevier; 1990. p. 137–212.

[54] Thomas OD, Soo KJWY, Peckham TJ, Kulkarni MP, Holdcroft S. Anion conducting poly(dialkyl benzimidazolium) salts. Polym Chem 2011;2:1641.

[55] Lampinen MJ, Fomino M. Analysis of free energy and entropy changes for half-cell reactions. J Electrochem Soc 1993;140(12):3537–46.

[56] Fang Z, Wang S, Zhang Z, Qiu G. The electrochemical Peltier heat of the standard hydrogen electrode reaction. Thermochim Acta 2008;473(1):40–4.